

Non-Boussinesq convection in porous media

Andres E. Rubiano and Marc A. Hesse *

Abstract Here we study the effect of non-Boussinesq effects on hydrothermal convection in porous media. This work is motivated by post-impact hydrothermal convection in the Chicxulub impact crater in Yucatán, Mexico. Post-impact hydrothermal simulation experiences very large temperature differences and significant changes in fluid properties. Studies of convection commonly employ the Boussinesq approximation which neglects density changes everywhere except the buoyancy term. To study the effect of this approximation in the presence of large density differences we compare convective fluxes from numerical simulations with and without the Boussinesq approximation. This study delves into the influence of temperature-dependent density on hydrothermal flow within porous media, drawing inspiration from the temperature profiles observed in the Chicxulub crater. These profiles showcase significant temperature variations, prompting the proposal of a non-Boussinesq approximation for the model. The weak formulation for the adimensional model is derived and finite element spaces are chosen according to the involved continuous spaces. Finally, we present numerical simulations using FEniCS for our new approach and the results are compared with the classical Boussinesq approximation.

Andres E. Rubiano
School of Mathematics, Monash University, 9 Rainforest Walk, 3163, Clayton, Victoria, Australia
e-mail: andres.rubianomartinez@monash.edu

Marc A. Hesse
Department of Geological Sciences, University of Texas at Austin, 23 San Jacinto Blvd, 78712,
Austin, Texas, United States
e-mail: mhesse@jsg.utexas.edu

* This report presents the results of a project undertaken by the first author at the Matrix Workshop *Instabilities in Porous Media*, April 3-23, 2024, under the supervision of the second author.

1 Motivation

65 million years ago, a city-sized asteroid collided with Earth, striking the shallow waters near the Yucatán Peninsula in the Gulf of Mexico (see Fig. 1). This catastrophic event created the Chicxulub crater, spanning 200 km in diameter. The significance of this event extends beyond its connection to the extensive extinction event of the Cretaceous–Paleogene era [10, 4]. The crater hosts a present-day deep microbial biosphere [5] (see Fig. 1) that presents a unique opportunity to study the role of post-impact hydrothermal systems in habitability across the solar system [12, 9]. This has led to several expeditions to study the crater and to drill into it to obtain data that helps to understand the evolution of this system. In addition, mathematical models and numerical simulations for the post-impact evolution have been developed to understand the longevity of the hydrothermal system [1, 2]. These models demonstrate that the temperature of the system experiences extreme temperature changes during the transient cooling and even the long-term steady state maintains large temperature differences, due to the size of the crater.

Many studies of convection in porous media invoke the so-called Boussinesq approximation that neglects density changes everywhere, except in the buoyancy term that drives convection. The reasoning behind the approximation is that even small density differences that have a negligible effect on mass and energy balance can destabilize the system and induce convective motion. This approximation is well accepted in cases with small temperature perturbations in typical groundwater systems. For hydrothermal systems, however, the assumptions for the approximation clearly break down. Due to the resulting large density changes, it is not clear if even the long-term steady state can be modeled by the Boussinesq approximation.

In this study, we will explore porous media convection with both the Boussinesq approximation and without it. The latter is significantly more complex because the mass and energy balances are fully coupled and have to be solved together using a Newton iteration. This is in contrast to the equations arising from the Boussinesq approximation, which allows sequential solution of the mass and energy balance equations. However, due to the advent of numerical platforms such as FeniCS it has become feasible to solve the coupled problem.

We begin by introducing the mathematical notation and defining key spaces pertinent to this type of equation. Subsequently, we outline the specific model under consideration, detailing its physical parameters, the scaling of the problems and the resulting dimensionless equations. The fully dimensionless model is then contrasted with the classical Boussinesq approximation. Following this, the weak formulation for both models is presented. Finally, we present numerical simulations illustrating the behavior of the proposed approaches.

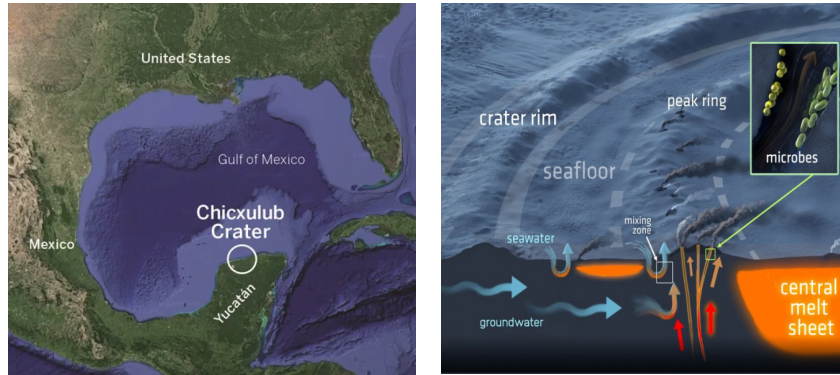


Fig. 1 Location of Chicxulub asteroid crater, taken from [11] (left), a three-dimensional cross-section of the hydrothermal system in the Chicxulub impact crater and its seafloor vents, taken from [8] (right).

2 Recurrent notation and Sobolev spaces

Let D be a polygonal Lipschitz bounded domain of \mathbb{R}^2 with boundary ∂D and $\mathbb{R}^+ := [0, \infty)$. In this work, we consider column vectors and the differential operators are applied row-wise. Hence, given a vector field $\zeta : D \rightarrow \mathbb{R}^2$ and a scalar function $T : D \times \mathbb{R}^+ \rightarrow \mathbb{R}$, we set the vector divergence $\nabla \cdot \zeta : D \rightarrow \mathbb{R}$ the scalar gradient $\nabla T : D \times \mathbb{R}^+ \rightarrow \mathbb{R}^2$ as:

$$\nabla \cdot \zeta := \sum_j \partial_j \zeta_j, \quad (\nabla T)_j := \partial_j T.$$

The component-wise inner product of two vector $\zeta, \xi \in \mathbb{R}^2$ is defined by $\zeta \cdot \xi := \sum_j \zeta_j \xi_j$. For $s \geq 0$, we denote the usual Hilbertian Sobolev space of scalar functions with domain D by $H^s(D)$, and denote their vector counterparts as $\mathbf{H}^s(D)$. The norm of $H^s(D)$ is denoted $\|\cdot\|_{s,D}$ and the corresponding semi-norm $|\cdot|_{s,D}$. We also use the convention $H^0(D) := L^2(D)$, where the inner product is defined by:

$$(T, \tau)_D := \int_D T \tau, \quad (\zeta, \xi)_D := \int_D \zeta \cdot \xi.$$

The space of vectors in $\mathbf{L}^2(D)$ with divergence in $L^2(D)$ is denoted $\mathbf{H}(\text{div}, D)$ and it is a Hilbert space equipped with the corresponding graph norm $\|\zeta\|_{\text{div}, D}^2 := \|\zeta\|_{0,D}^2 + \|\text{div} \zeta\|_{0,D}^2$. On the other hand, let n be the outward unit normal vector to ∂D , the classical Green Formula is given by:

$$(\zeta, \nabla T)_D + (\nabla \cdot \zeta, T)_D = \int_{\partial D} (\zeta \cdot n) T \quad \forall T \in H^1(D). \quad (1)$$

3 The model problem

In a porous media with porosity ϕ , the conservation of mass and energy are given by:

$$\phi \frac{\partial \rho_f(T)}{\partial t} + \nabla \cdot (\rho_f(T) \mathbf{q}) = 0, \quad (2)$$

$$\frac{\partial H(T)}{\partial t} + \nabla \cdot (\mathbf{q} \rho_f(T) h_f(T) - \bar{\kappa} \nabla T) = 0. \quad (3)$$

where ρ_f is the fluid density, $\bar{\kappa} = \phi \kappa_f + (1 - \phi) \kappa_s$ is the effective thermal conductivity of the saturated porous medium and H is the total enthalpy of the system. The specific enthalpies of the phases are given by $h_i = c_i(T - T_0)$, where c_i 's are the heat capacities of the fluid and solid phases, respectively. Therefore, the total enthalpy of the system is given by:

$$H(T) = \phi \rho_f(T) h_f(T) + (1 - \phi) \rho_s h_s(T), \quad (4)$$

where ρ_s is the density of the solid. The equations above are completed by the following two constitutive laws:

$$\mathbf{q} = -\frac{k}{\mu} (\nabla p + \rho_f(T) g \hat{\mathbf{z}}), \quad (5)$$

$$\rho_f = \rho_0(1 + \beta(T - T_0)), \quad (6)$$

where μ is the viscosity of the fluid and g is the gravitational acceleration. Equation (5) is Darcy's law for the pore fluid and (6) is the equation of state for the density as a function of temperature. For the purpose of this initial study, we assume a simple linear relationship with β as the thermal expansivity of the fluid. Eventually, steamtables should be used to evaluate all fluid properties as a function of T and p .

We consider flow in a simple rectangular domain Ω fixed in the (x, z) axis (see Fig. 2), of depth D and length L with initial temperature $T = T_{\text{initial}}$. No mass and energy flux conditions are imposed on the side boundaries, $(\partial\Omega)_{\text{walls}}$. The bottom boundary, $(\partial\Omega)_{\text{bottom}}$, has a fixed boundary temperature $T(x, 0) = T_{\text{bottom}}$ and no mass flux.

To allow for the expansion of the fluid due to non-Boussinesq effects top of the domain is open and the pressure is prescribed on $(\partial\Omega)_{\text{top}}$ as zero. For the energy we prescribe an outflow/inflow boundary condition at the top $(\partial\Omega)_{\text{top}}$, given by:

$$\begin{cases} \mathbf{q} \cdot \hat{\mathbf{z}} > 0: & \nabla T \cdot \hat{\mathbf{z}}|_{z=D} = 0, \\ \mathbf{q} \cdot \hat{\mathbf{z}} \leq 0: & T(x, D) = T_{\text{top}}. \end{cases}$$

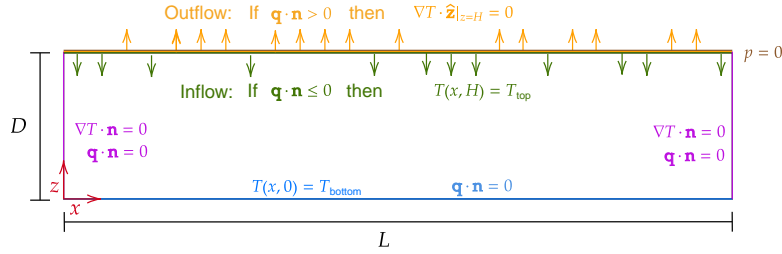


Fig. 2 Illustration of the domain with the boundary and initial conditions.

The physical parameters for this model are taken from Table 1 which are motivated by the conditions on the impact zone of the Chicxulub crater. These parameters can be used to non-dimensionalize the variables as shown in Table 2. Due to the temperature-dependent density we have the following dimensionless heat content functions:

$$\bar{\rho c}(T) = \frac{\phi \rho_f(T) c_f + (1 - \phi) \rho_s c_s}{\bar{\rho c}_0} \quad \text{with} \quad \bar{\rho c}_0 = \phi \rho_0 c_f + (1 - \phi) \rho_s c_s,$$

where the latter is the initial heat content. This motivates the definition of the following dimensionless groups:

$$\text{Pe} = \frac{q_c D}{\bar{\alpha}}, \quad \Gamma = \frac{\rho_0 c_f}{\bar{\rho c}_0}, \quad \Theta = \beta \Delta T,$$

known as the Péclet number, thermal inertia, and thermal expansion, respectively.

3.1 The simplified problem: Boussinesq approximation

In the classical Boussinesq approximation, the density is defined as a constant ρ_0 everywhere except in the buoyancy term in Darcy’s law. Therefore, the dimensionless governing equations are reduced to:

$$\nabla \cdot \mathbf{q} = 0, \tag{7a}$$

$$\frac{\partial T}{\partial t} + \nabla \cdot \left(\Gamma \mathbf{q} T - \frac{1}{\text{Pe}} \nabla T \right) = 0, \tag{7b}$$

$$-(\nabla p + \rho(T) \hat{\mathbf{z}}) - \mathbf{q} = 0, \tag{7c}$$

where we have dropped the primes and the dimensionless density is given by $\rho(T) = 1 - \Theta T$. Note that the flow field in the Boussinesq approximation is incompressible, as indicated by (7a). This allows the simulation of convection in closed domains

Table 1 Parameters values

parameter	value	units
D	500	m
k	10^{-14}	m^2
μ	10^{-3}	Pa s
ϕ	0.2	-
ρ_0	10^3	m^3/kg
ρ_s	2300	m^3/kg
c_f	4184	J/kg
c_s	1000	J/kg
T_0	20	$^\circ\text{C}$
T_b	100	$^\circ\text{C}$
ΔT	$T_b - T_0$	$^\circ\text{C}$
β	-210×10^{-6}	$1/^\circ\text{C}$

Table 2 Dimensionless variables

dim.-less variable	definition
T'	$\frac{T-T_0}{\Delta T}$
\mathbf{x}'	$\frac{\mathbf{x}}{H}$
\mathbf{q}'	$\frac{\mathbf{q}\mu}{k\rho_0 g}$
t'	$\frac{t q_c}{H}$
p'	$\frac{p}{\rho_0 g H}$
$\rho'(T')$	$\frac{\rho(T)}{\rho_0}$
$\bar{\rho}c'(T')$	$\frac{\bar{\rho}c(T)}{\bar{\rho}c_0}$
$h'_f(T')$	$\frac{h_f(T)}{c_f \Delta T} = T'$
$h'_s(T')$	$\frac{h_s(T)}{c_f \Delta T} = \frac{c_s}{c_f} T'$
$H'(T')$	$\frac{H(T)}{\bar{\rho}c_0 \Delta T} = \bar{\rho}c'(T')T'$

because overall volume changes of the fluid are neglected. The elliptic nature of (7a) and (7c) also allows a staggered solution where \mathbf{q} and T fields are computed in a sequential scheme.

3.2 The fully-coupled problem: Non-Boussinesq approximation

For the fully-coupled problem, the mass flux, $\zeta = \rho(T)\mathbf{q}$, rather than the volumetric flux given by Darcy's law is the natural flux field. Similarly it is more natural to solve for the enthalpy, H , rather than the temperature, T . The dimensionless fully-coupled equations in terms of ζ and H can then be written as:

$$\phi \frac{\partial \rho(T)}{\partial t} + \nabla \cdot \zeta = 0, \quad (8a)$$

$$\frac{\partial H(T)}{\partial t} + \nabla \cdot \left(\Gamma \zeta T - \frac{1}{\text{Pe}} \nabla T \right) = 0, \quad (8b)$$

$$-(\nabla p + \rho(T)\hat{\mathbf{z}}) - \frac{1}{\rho(T)} \zeta = 0, \quad (8c)$$

where again we have dropped the primes from the dimensionless equations. The dimensionless enthalpy and density are given by $H(T) = -\phi \Theta \Gamma T^2 + T$ and $\rho(T) = 1 - \Theta T$, respectively. We note that (8b) is written in terms of both H and T . The definition of the enthalpy above provides the necessary non-linear algebraic constraint.

4 Weak formulation for the proposed models

In view of the boundary conditions provided in Fig. 2 and the dimensional parameters given in Table 2, we define the following Hilbert spaces:

$$\begin{aligned} H_D^1(\Omega) &:= \{ \tau \in H^1(\Omega) : \tau = 1 \text{ on } (\partial\Omega)_{\text{bottom}}, \tau = 0 \text{ on } (\partial\Omega)_{\text{top}} \}, \\ \mathbf{H}_N(\text{div}, \Omega) &:= \{ \xi \in \mathbf{H}(\text{div}, \Omega) : \xi \cdot \mathbf{n} = 0 \text{ on } (\partial\Omega)_{\text{bottom}} \cup (\partial\Omega)_{\text{walls}} \}. \end{aligned}$$

In addition, we perform the following time discretization for the terms that involve time derivatives as follows:

$$\frac{\partial T}{\partial t} = \frac{T_n - T_{n-1}}{\Delta t}, \quad \frac{\partial H(T)}{\partial t} = \frac{H(T_n) - H(T_{n-1})}{\Delta t} \quad \text{and} \quad \frac{\partial \rho(T)}{\partial t} = \frac{\rho(T_n) - \rho(T_{n-1})}{\Delta t}.$$

Therefore, Eq. (1) and the boundary conditions lead to the following weak formulation for the Boussinesq approximation: For given $T_{n-1} \in L^2(\Omega)$, find $(T_n, \mathbf{q}, p) \in H_D^1(\Omega) \times \mathbf{H}_N(\text{div}, \Omega) \times L^2(\Omega)$ such that:

$$\frac{1}{\Delta t} \int_{\Omega} T_n \tau + \Gamma \int_{\Omega} (\mathbf{q} \cdot \nabla T_n) \tau + \frac{1}{\text{Pe}} \int_{\Omega} \nabla T_n \cdot \nabla \tau = \frac{1}{\Delta t} \int_{\Omega} T_{n-1} \tau, \quad (9a)$$

$$\int_{\Omega} \mathbf{q} \cdot \mathbf{q}' - \int_{\Omega} p(\nabla \cdot \mathbf{q}') = - \int_{\Omega} \rho(T_n) \hat{\mathbf{z}} \cdot \mathbf{q}', \quad (9b)$$

$$- \int_{\Omega} (\nabla \cdot \mathbf{q}) q = 0, \quad (9c)$$

for all $\tau \in H_D^1(\Omega)$, $\mathbf{q}' \in \mathbf{H}_N(\text{div}, \Omega)$ and $q \in L^2(\Omega)$. Note that the second and third rows in 9 form a classical perturbed saddle-point problem which appears often in the mixed formulations literature (see e.g. [3]), in this case, with a non-linear coupling term in the right-hand side and the first row corresponds to the classical weak formulation for divergence-free advection-reaction-diffusion equation where the coupling is shown in the advection term.

On the other hand, the weak form for the full non-Boussinesq approximation reads: For given $T_{n-1} \in L^2(\Omega)$, find $(T_n, \zeta, p) \in H_D^1(\Omega) \times \mathbf{H}_N(\text{div}, \Omega) \times L^2(\Omega)$ such that:

$$\frac{1}{\Delta t} \int_{\Omega} H(T_n) \tau + \Gamma \int_{\Omega} ((\nabla \cdot \zeta) T_n + \zeta \cdot \nabla T_n) \tau + \frac{1}{\text{Pe}} \int_{\Omega} \nabla T_n \cdot \nabla \tau = \frac{1}{\Delta t} \int_{\Omega} H(T_{n-1}) \tau, \quad (10a)$$

$$\int_{\Omega} \frac{1}{\rho(T_n)} \zeta \cdot \xi - \int_{\Omega} p(\nabla \cdot \xi) = - \int_{\Omega} \rho(T_n) \hat{\mathbf{z}} \cdot \xi, \quad (10b)$$

$$- \int_{\Omega} (\nabla \cdot \zeta) q = \frac{\phi}{\Delta t} \int_{\Omega} (\rho(T_n) - \rho(T_{n-1})) q, \quad (10c)$$

for all $\tau \in H_D^1(\Omega)$, $\xi \in \mathbf{H}_N(\text{div}, \Omega)$ and $q \in L^2(\Omega)$. In this case, the second and third rows in (10) form a classical perturbed saddle-point problem with full non-linear coupling right-hand sides and non-linear mass term. For the first row, a non-linearity appears with the mass term together with a coupling via the advection term. This means that the continuous analysis of this equation will involve additional work.

The continuous analysis of these two equations can be proposed as an additional project (see e.g. [7, 6]). In this study, we only focus on defining the model problem and its implementation with finite elements using FEniCS, ensuring that the simulations yield results faithful to real-world phenomena.

5 Numerical simulations

For the FEM spaces, we define classical continuous Lagrange elements of degree $k = 1$ for the space $H^1(\Omega)$, Brezzi–Douglas–Marini (BDM) elements of degree $k = 1$ for $\mathbf{H}(\text{div}, \Omega)$ and Discontinuous Lagrange elements of degree $k = 0$ for $L^2(\Omega)$.

The experiments presented are set with $\phi = 0.2$, $\Gamma = 1.56$, and $Pe = 3053.42$; these values correspond to the parameters shown in Table 1. Since the parameter Θ is controlling the temperature-dependent density by the relation $\rho(T) = 1 - \Theta T$, we introduce a variation in this parameter given by the values: $\Theta = 0.02, 0.2, 0.4$. The discrete domain is set as the rectangle $[0, 3] \times [0, 1]$ discretized by a triangle-made “crossed” grid of size 150×50 . The initial condition for temperature is set as:

$$T(x, 0) = \begin{cases} 0 & \text{if } x \leq 1.5, \\ 0.1 & \text{if } x > 1.5. \end{cases}$$

In addition, we compute the flux on the system for each time step given by:

$$F_{\text{top}}(t) = \int_0^3 \Gamma \mathbf{q} T - \frac{1}{Pe} \nabla T, \quad \text{and} \quad F_{\text{top}}(t) = \int_0^3 \Gamma \zeta T - \frac{1}{Pe} \nabla T,$$

for Boussinesq and non-Boussinesq models, respectively.

Small values of Θ set the density $\rho(T)$ close to ρ_0 . Hence, no visible changes are expected between the two models as shown in Fig. 3. On the other hand, increasing this value, apart from the fact that the instability grows, the density changes along with the formation of a fingering pattern. Moreover, there are clear changes in the flux present in the top layer as shown in Fig. 4 and Fig. 5.

6 Conclusions

We showed via numerical simulations that the proposed model for hydrothermal flow within porous presents evident differences with the classical Boussinesq ap-

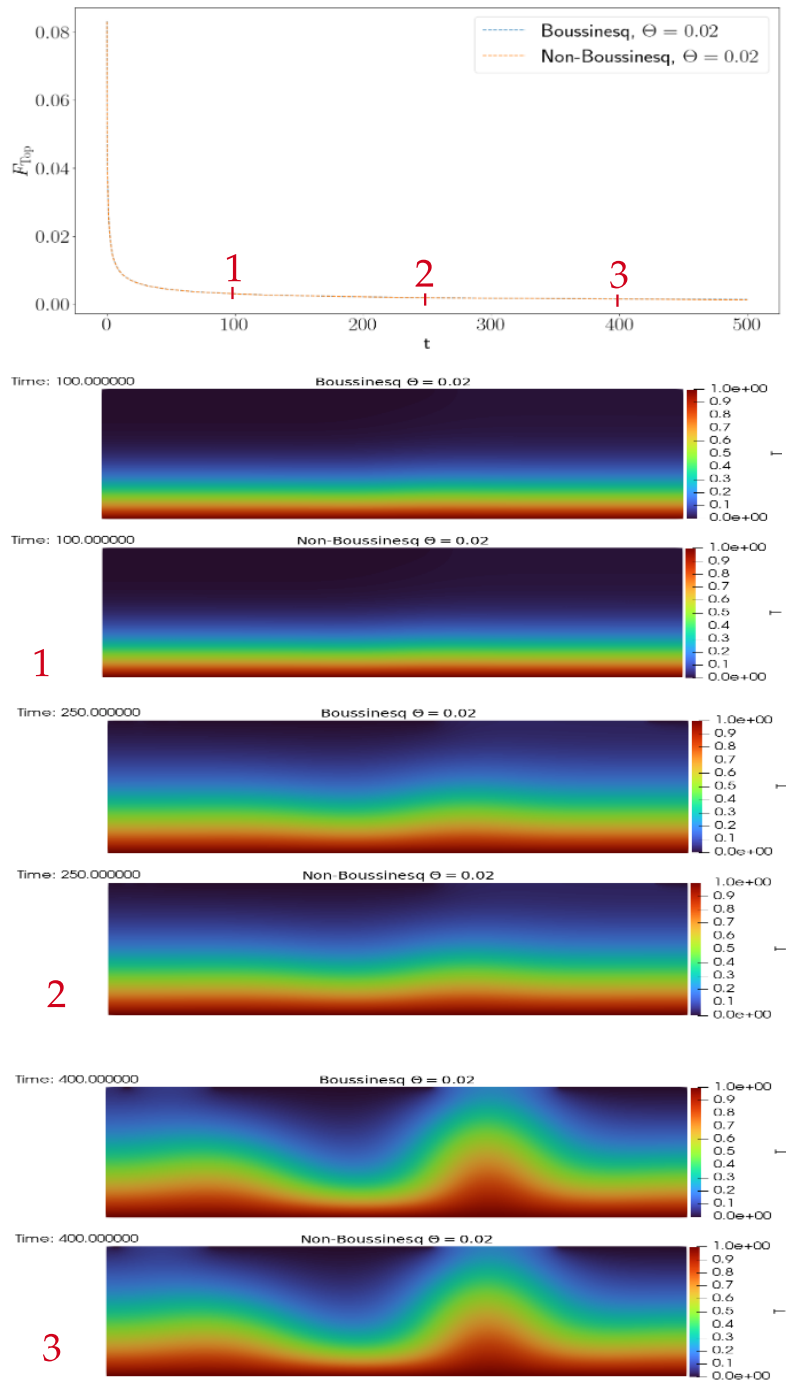


Fig. 3 Snapshots of F_{top} and the associated temperature at different time steps for $\Theta = 0.02$.

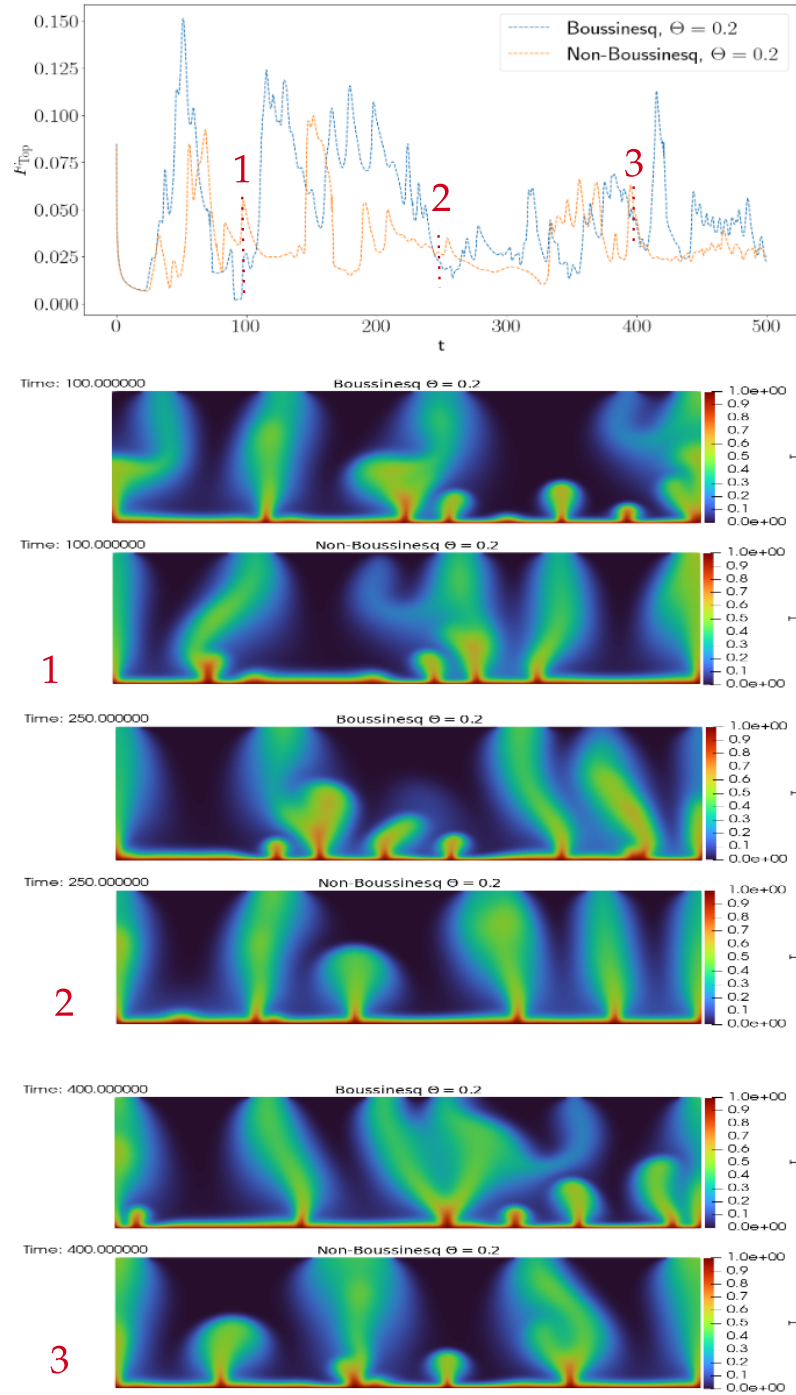


Fig. 4 Snapshots of F_{top} and the associated temperature at different time steps for $\Theta = 0.2$.

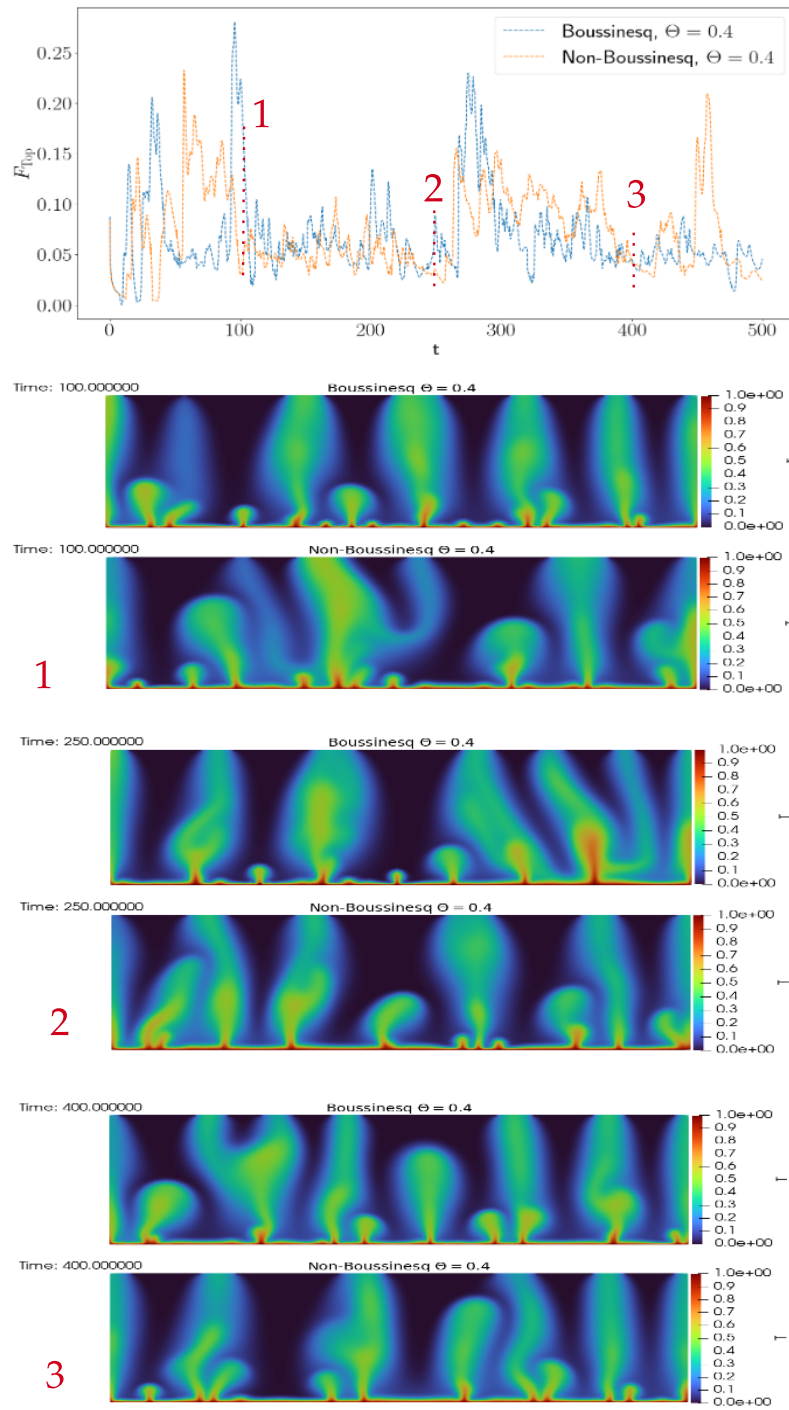


Fig. 5 Snapshots of F_{top} and the associated temperature at different time steps for $\Theta = 0.4$.

proximation for high perturbations on density. This will motivate the usage of non-Boussinesq models for systems that present big temperature changes. In future work, the well-posedness of this model will be explored, and the reliability of this model will be tested on different applications and validated with the available data.

Acknowledgements The second author would like to express gratitude to Ricardo Ruiz-Baier for generously providing a simplified FEniCS script, which served as the starting point for the numerical simulations showcased in this work. We thank the mathematical research institute MATRIX in Australia where part of this research was performed.

References

1. Abramov, O., Kring, D.: Numerical modeling of hydrothermal activity at the Chicxulub crater. *Meteoritics and Planetary Science* **42**, 93–112 (2007). DOI 10.1111/j.1945-5100.2007.tb00220.x
2. Alfred, S.M., Gulick, S.P.S., Hesse, M.A., McCall, N.T.: Modeling of the Post-Impact Hydrothermal System at the Chicxulub Crater — [agu.confex.com](https://agu.confex.com/agu/fm23/meetingapp.cgi/Paper/1320418). <https://agu.confex.com/agu/fm23/meetingapp.cgi/Paper/1320418> (2024)
3. Boffi, D., Brezzi, F., Fortin, M.: *Mixed Finite Element Methods and Applications*, vol. 44. Springer (2013). DOI 10.1007/978-3-642-36519-5
4. Christeson, G.L., Morgan, J.V., Gulick, S.P.S.: Mapping the Chicxulub impact stratigraphy and peak ring using drilling and seismic data. *Journal of Geophysical Research: Planets* **126**, e2021JE006938 (2021). DOI 10.1029/2021JE006938
5. Cockell, C.S., Schaefer, B., Wuchter, C., Coolen, M.J.L., Grice, K., Schnieders, L., Morgan, J.V., Gulick, S.P.S., Wittmann, A., Lofi, J., Christeson, G.L., Kring, D.A., Whalen, M.T., Bralower, T.J., Osinski, G.R., Claeys, P., Kaskes, P., de Graaff, S.J., Déhais, T., Goderis, S., Hernandez Becerra, N., Nixon, S., I.I.E.S.: Shaping of the present-day deep biosphere at Chicxulub by the impact catastrophe that ended the Cretaceous. *Frontiers in Microbiology* **12** (2021). DOI 10.3389/fmicb.2021.668240
6. Colmenares, E., Gatica, G.N., Moraga, S.: A Banach spaces-based analysis of a new fully-mixed finite element method for the Boussinesq problem. *ESAIM: M2AN* **54**, 1525–1568 (2020). DOI 10.1051/m2an/2020007
7. Colmenares, E., Gatica, G.N., Moraga, S., Ruiz-Baier, R.: A fully-mixed finite element method for the steady state Oberbeck–Boussinesq system. *The SMAI Journal of Computational Mathematics* **6**, 125–157 (2020). DOI 10.5802/smai-jcm.64
8. Kring, D.A.: The Chicxulub Impact Crater: Producing a Cradle of Life in the Midst of a Global Calamity — [lpi.usra.edu](https://www.lpi.usra.edu/publications/newsletters/lpib/new/the-chicxulub-impact-crater-producing-a-cradle-of-life-in-the-midst-of-a-global-calamity/). <https://www.lpi.usra.edu/publications/newsletters/lpib/new/the-chicxulub-impact-crater-producing-a-cradle-of-life-in-the-midst-of-a-global-calamity/> (2021).
9. Le Ber, E., Loggia, D., Denchik, N., Lofi, J., Kring, D.A., Sardini, P., Siitari-Kauppi, M., Pezard, P., Olivier, G., Party, I.I.E.S.: Petrophysics of Chicxulub impact crater’s peak ring. *Journal of Geophysical Research: Solid Earth* **127**, e2021JB023801 (2022). DOI 10.1029/2021JB023801
10. Morgan, J.V., Gulick, S.P.S., Bralower, T., Chenot, E., Christeson, G., Claeys, P., Cockell, C., Collins, G.S., Coolen, M.J.L., Ferrière, L., Gebhardt, C., Goto, K., Jones, H., Kring, D.A., Ber, E.L., Lofi, J., Long, X., Lowery, C., Mellett, C., Ocampo-Torres, R., Osinski, G.R., Perez-Cruz, L., Pickersgill, A., Poelchau, M., Rae, A., Rasmussen, C., Rebolledo-Vieyra, M., Riller, U., Sato, H., Schmitt, D.R., Smit, J., Tikoo, S., Tomioka, N., Urrutia-Fucugauchi, J., Whalen, M., Wittmann, A., Yamaguchi, K.E., Zylberman, W.: The formation of peak rings in large impact craters. *Science* **354**, 878–882 (2016). DOI 10.1126/science.aah6561

11. Parks, J.: Chicxulub Crater dust confirms cause of dinosaurs' extinction — astronomy.com. <https://www.astronomy.com/science/asteroid-dust-found-at-chicxulub-crater-confirms-cause-of-dinosaurs-extinction/> (2023).
12. Rae, A.S.P., Collins, G.S., Morgan, J.V., Salge, T., Christeson, G.L., Leung, J., Lofi, J., Gulick, S.P.S., Poelchau, M., Riller, U., Gebhardt, C., Grieve, R.A.F., Osinski, G.R., Scientists, I.I.E...: Impact-induced porosity and microfracturing at the Chicxulub impact structure. *Journal of Geophysical Research: Planets* **124**, 1960–1978 (2019). DOI 10.1029/2019JE005929.